Continental Shelf Research 29 (2009) 911–926

Contents lists available at ScienceDirect

Continental Shelf Research

journal homepage: www.elsevier.com/locate/csr

Wave-induced steady streaming, mass transport and net sediment transport in rough turbulent ocean bottom boundary layers

Lars Erik Holmedal *, Dag Myrhaug

Department of Marine Technology, Norwegian University of Science and Technology, NO-7491 Trondheim, Norway

ARTICLE INFO

Article history:
Received 3 December 2008
Accepted 27 January 2009
Available online 10 February 2009

Keywords:
Oscillatory boundary layer
Mass transport
Streaming
Waves
Sediment transport

ABSTRACT

The interaction between two important mechanisms which causes streaming has been investigated by numerical simulations of the seabed boundary layer beneath both sinusoidal waves and Stokes second order waves, as well as horizontally uniform bottom boundary layers with asymmetric forcing. These two mechanisms are streaming caused by turbulence asymmetry in successive wave half-cycles (beneath asymmetric forcing), and streaming caused by the presence of a vertical wave velocity within the seabed boundary layer as earlier explained by Longuet-Higgins. The effect of wave asymmetry, wave length to water depth ratio, and bottom roughness have been investigated for realistic physical situations. The streaming induced sediment dynamics near the ocean bottom has been investigated; both the resulting suspended load and bedload are presented. Finally, the mass transport (wave-averaged Lagrangian velocity) has been studied for a range of wave conditions. The streaming velocities beneath sinusoidal waves (Longuet-Higgins streaming) is always in the direction of wave propagation, while the streaming velocities in horizontally uniform boundary layers with asymmetric forcing are always negative. Thus the effect of asymmetry in second order Stokes waves is either to reduce the streaming velocity in the direction of wave propagation, or, for long waves relative to the water depth, to induce a streaming velocity against the direction of wave propagation. It appears that the Longuet-Higgins streaming decreases as the wave length increases for a given water depth, and the effect of wave asymmetry can dominate, leading to a steady streaming against the wave propagation. Furthermore, the asymmetry of second order Stokes waves reduces the mass transport (wave-averaged Lagrangian velocity) as compared with sinusoidal waves. The boundary layer streaming leads to a wave-averaged transport of suspended sediments and bedload in the direction of wave propagation.

1. Introduction

In coastal waters of intermediate or shallow water depths the surface waves induce water particle trajectories from the free surface to the bottom, dominating the flow in the water column. Near the bottom an oscillating boundary layer is formed because of the bottom friction. Inside this boundary layer, the wave-induced forcing is responsible for the transport of sea bed material either as bedload or as suspended load. This material includes sediments, chemical compounds, as well as biological material such as fish larvae.

Ocean surface waves are progressive, and for finite water depths the near-bottom water particle trajectories are ellipses where the horizontal axis is much larger than the vertical axis. Thus a small vertical wave velocity exists in the flow, and the existence of this vertical wave velocity gives rise to a weak mass transport within the oscillatory bottom boundary layer. This happens because the vorticity and turbulence created within the oscillating boundary layer are transported upwards from the bottom with time. Hence a weak vorticity exists in a layer much thicker than the oscillating boundary layer (Batchelor, 1967). As a result, the vertical and horizontal velocity components are not 90° out of phase within this layer (as they are in potential flow), and the vertical wave velocity combines with the horizontal wave velocity through the convective terms in the governing boundary layer equations, giving rise to a non-zero wave-averaged drift within the oscillatory boundary layer. This effect is caused by the bottom friction and wave action, and is commonly referred to as steady streaming. This streaming phenomenon for oscillating bottom boundary layers beneath gravity waves was first explained by Longuet-Higgins (1953). However, steady streaming also arises because of wave asymmetry, as described in detail by Scandura (2007) and Davies and Li (1997) for flows in the transitional laminar to turbulent regime and flows in the rough turbulent regime, respectively. This phenomenon was first measured in an oscillating water tunnel by Ribberink and Al-Salem (1995). As

* Corresponding author.
E-mail address: lars.erik.holmedal@ntnu.no (L.E. Holmedal).

0278-4343/$ - see front matter © 2009 Elsevier Ltd. All rights reserved.
doi:10.1016/j.csr.2009.01.012

pointed out by Scandura (2007) the effect of wave asymmetry is particularly important in shallow waters. However, as explained by Longuet-Higgins (1953), the steady streaming velocity will also be present in realistic near-bottom flows beneath symmetric waves.

Previous works dealing with steady streaming within ocean bottom boundary layers, among others (Trowbridge and Madsen, 1984; Brøker, 1985; Justesen, 1988; Hsu and Ou, 1994; Deigaard et al., 1999) have considered boundary layer models where the horizontal gradient operator in the convective term has been approximated by $\partial/\partial x = -(1/c_p)\partial/\partial t$ (c_p being the wave celerity, x the horizontal direction and t the time). Johns (1977) used a one-equation turbulence model in two spatial dimensions to investigate the Eulerian mean velocity beneath sinusoidal waves propagating over a flat bottom. Unfortunately, the boundary conditions applied on the upper part of the boundary layer are not realistic for describing the steady streaming in ocean bottom boundary layers. Chowdhury et al. (1997) used a one-equation turbulence closure to obtain the steady streaming velocity under second order Stokes waves in two spatial dimensions. The asymmetry of the boundary layer forcing beneath ocean waves, caused by the second harmonic component of the velocity at the outer edge of the boundary layer, was also taken into account by Trowbridge and Madsen (1984) and by Deigaard et al. (1999). However, the Stokes drift within the boundary layer was not included in any of these works. Longuet-Higgins (1953) was the first to point out that the Stokes drift must be included to obtain the mass transport, but he only considered the symmetric (sinusoidal) boundary layer forcing.

Longuet-Higgins (1953) showed that for laminar oscillatory bottom boundary layer flows with sinusoidal forcing, the mass transport is in the same direction as the wave propagation. This result was qualitatively confirmed in measurements by Russel and Osorio (1958) and Collins (1963) for low Reynolds number (i.e. nearly laminar) flow over a smooth bottom. However, Collins' measurements revealed that the steady streaming velocity was reduced in magnitude as the Reynolds number was increased, i.e. as the flow became more turbulent. This was confirmed in wave flume experiments for rough bottoms conducted by Bijker et al. (1974) and van Doorn (1981). Trowbridge and Madsen (1984) showed that the inclusion of a time dependent eddy viscosity in the boundary layer model was essential to capture the reduced mass transport for turbulent flows. This was later confirmed by Brøker (1985), who used the model by Fredsøe (1984) to calculate the mass transport for a horizontally uniform oscillating boundary layer flow. Trowbridge and Madsen (1984) also showed that when the boundary layer is subjected to asymmetric forcing, the steady streaming velocity can be against the direction of wave propagation for very long waves; Deigaard et al. (1999) found similar results for long bound waves. Negative steady streaming velocities are also found in oscillating bottom boundary layers subjected to horizontally uniform forcing by Ribberink and Al-Salem (1995), rough bottom; Davies and Li (1997), rough bottom; Holmedal and Myrhaug (2006), rough bottom; Scandura (2007), smooth bottom. A broader review of steady streaming can be found in Mei (1989), Trowbridge and Madsen (1984), and Riley (2001).

Realistic conditions in the ocean imply that the bottom is rough (consisting of sand) and that the bottom boundary layer flow is turbulent. Hence a turbulence model which accounts for the bottom roughness is required. Here a standard high Reynolds number $k-\varepsilon$ model is chosen in conjunction with a logarithmic wall law near the bottom. This model with its standard model coefficients, was recommended by Launder and Spalding (1974) for plane jets, mixing layers, and unidirectional steady flow close to the wall; more recently it has also been applied successfully to predict turbulent oscillating boundary layer flows over rough bottoms. In particular Justesen (1991) and, more recently, Holmedal et al. (2003, Appendix A) successfully applied the $k-\varepsilon$ model to predict the turbulent oscillating boundary layer flow over a rough flat bottom. The corresponding measurements by Jensen et al. (1989, Test number 13) were well predicted; this included the instantaneous boundary layer velocity, shear stress and turbulent kinetic energy profiles, as well as the bottom friction velocity through the wave cycle. Recently, Holmedal and Myrhaug (2006) applied the standard high Reynolds number $k-\varepsilon$ model to predict periodic boundary layer flows due to asymmetric forcing for horizontally uniform flows. The predictions agree with the experimental data provided by Ribberink and Al-Salem (1995). Therefore, it is expected that the $k-\varepsilon$ model will lead to satisfactory predictions when applied to investigate the steady streaming and mass transport velocities near the ocean bottom.

This paper will focus on the interaction between two important mechanisms causing streaming: the first is streaming caused by turbulence asymmetry in successive wave half-cycles (beneath asymmetric boundary layer forcing); the second is streaming caused by the presence of the vertical wave velocity within the seabed boundary layer as explained by Longuet-Higgins (1953). The effect of wave asymmetry, the wave length to water depth ratio, and the bottom roughness have been investigated for realistic physical situations. The interaction between these two streaming mechanisms is essential because it addresses important differences between oscillatory flows in closed tunnels and real wave boundary layers under progressive waves. It also helps explaining the different streaming mechanisms beneath long waves and short waves, and beneath weak and strong wave asymmetries. Moreover, the mass transport (i.e. the wave-averaged Lagrangian velocity) beneath second order Stokes waves has been investigated for the first time. To the authors knowledge, no results from such a systematic study are available in the open literature. This is also the case for the results on the streaming induced sediment dynamics near the ocean bottom under realistic physical conditions, where both the suspended load and bedload have been investigated. The streaming mechanisms and resulting sediment dynamics have been investigated by numerical simulations of the bottom boundary layer beneath both progressive sinusoidal and Stokes second order waves, as well as horizontally uniform bottom boundary layers with asymmetric forcing.

2. Model formulation

2.1. Governing equations

Wave-induced mass transport in bottom boundary layers over an infinitely long flat bottom is considered. The horizontal coordinate at the bottom is given as x, whilst the vertical coordinate z gives the distance from the bottom. The bottom is fixed at $z = z_0 = k_N/30$, where k_N is the equivalent Nikuradse roughness. The limits of the horizontal coordinate x is such that $x = 0$ at the start of the wave length, and $x = \lambda$ at the end of the wave length. For intermediate and shallow water depths, the water particle trajectories are ellipses where the horizontal axis is much larger than the vertical axis. Hence the boundary layer approximation applies, and the simplified Reynolds-averaged equations for conservation of the mean momentum and mass become

$$\frac{\partial u}{\partial t} + \frac{\partial (u^2)}{\partial x} + \frac{\partial (uw)}{\partial z} = -\frac{1}{\rho}\frac{\partial p}{\partial x} + \frac{\partial}{\partial z}\left(\nu_T \frac{\partial u}{\partial z}\right) \tag{1}$$

$$\frac{\partial u}{\partial x} + \frac{\partial w}{\partial z} = 0 \tag{2}$$

where u is the horizontal velocity component, w is the vertical velocity component, p is the pressure, ρ is the density of the water, and ν_T is the kinematic eddy viscosity. The turbulence closure is provided by a $k-\varepsilon$ model. Subjected to the boundary layer approximation, these transport equations are given by (see e.g. Rodi, 1993)

$$\frac{\partial k}{\partial t}+\frac{\partial(uk)}{\partial x}+\frac{\partial(wk)}{\partial z}=\frac{\partial}{\partial z}\left(\frac{\nu_T}{\sigma_k}\frac{\partial k}{\partial z}\right)+\nu_T\left(\frac{\partial u}{\partial z}\right)^2-\varepsilon \tag{3}$$

$$\frac{\partial \varepsilon}{\partial t}+\frac{\partial(u\varepsilon)}{\partial x}+\frac{\partial(w\varepsilon)}{\partial z}=\frac{\partial}{\partial z}\left(\frac{\nu_T}{\sigma_\varepsilon}\frac{\partial \varepsilon}{\partial z}\right)+c_{\varepsilon 1}\frac{\varepsilon}{k}\nu_T\left(\frac{\partial u}{\partial z}\right)^2-c_{\varepsilon 2}\frac{\varepsilon^2}{k} \tag{4}$$

where k is the turbulent kinetic energy and ε is the turbulent dissipation rate. Here Eq. (2) has been applied to write Eqs. (1), (3), and (4) in conservative form. The kinematic eddy viscosity is given by

$$\nu_T=c_1\frac{k^2}{\varepsilon} \tag{5}$$

The standard values of the model constants have been adopted, i.e. $(c_1, c_{\varepsilon 1}, c_{\varepsilon 2}, \sigma_k, \sigma_\varepsilon)=(0.09, 1.44, 1.92, 1.00, 1.30)$.

The instantaneous dimensionless bedload transport Φ is a function of the instantaneous dimensionless sea bed shear stress (Shields parameter) θ and is given by a formula by Nielsen (1992)

$$\Phi=12\theta^{1/2}(\theta-\theta_c)\frac{\theta}{|\theta|} \tag{6}$$

where

$$\Phi=\frac{q_b}{(g(s-1)d_{50}^3)^{1/2}} \tag{7}$$

$$\theta=\frac{\tau_b}{\rho g(s-1)d_{50}} \tag{8}$$

Here q_b is the instantaneous dimensional bedload transport, τ_b is the dimensional instantaneous sea bed shear stress, g is the gravity acceleration, $s=2.65$ is the density ratio between the bottom sediments and the water, ρ is the water density, and d_{50} is the median grain size diameter. The critical Shields parameter $\theta_c=0.05$ must be exceeded for bedload transport to take place.

By using the boundary layer approximation, the equation for the sediment concentration c is written as

$$\frac{\partial c}{\partial t}+u\frac{\partial c}{\partial x}+(w-w_s)\frac{\partial c}{\partial z}=\frac{\partial}{\partial z}\left(\varepsilon_s\frac{\partial c}{\partial z}\right) \tag{9}$$

$$\varepsilon_s=\nu_T+\nu \tag{10}$$

Here ε_s is the sediment diffusivity, w_s is the settling velocity of the median sand grains in still water, and ν is the laminar kinematic viscosity of water. Here the laminar viscosity has been included in the sediment diffusivity in order to stabilize the numerical scheme; this model is described in more detail in Holmedal et al. (2004).

2.2. Simplification of equations

In order to simplify the mathematical solution to Eqs. (1)–(4) and (9) the relation $\partial/\partial x=-(1/c_p)\partial/\partial t$ is applied. This is an approximation which is only valid for weakly decreasing waves (i.e. the wave height decay over a wave length due to the energy dissipation is small); this will be discussed further in conjunction with Eq. (14), and in Section 3. This approximation leads to the two-dimensional boundary layer equations (i.e. Eqs. (1), (3), (4), and (9)) reducing to spatially one-dimensional equations. Physically this transformation implies a mapping from two spatial dimensions to one spatial dimension. The length of the physical two-dimensional space is one wave length, and the height is $z_{max}-z_0$ in one dimension. The results obtained in one dimension can be mapped back to the physical two-dimensional space. This is useful when for, e.g., calculating the particle trajectories.

As a consequence of this simplification the vertical velocity component is found from the continuity equation and is evaluated as

$$w=-\int_{z=z_0}^{z}\frac{\partial u}{\partial x}\,dz=\frac{1}{c_p}\int_{z=z_0}^{z}\frac{\partial u}{\partial t}\,dz \tag{11}$$

and inserted into Eqs. (1), (3), (4), and (9). Here $w=0$ at $z=z_0$ has been utilized (see Eq. (15)).

The relation $\partial/\partial x=-(1/c_p)\partial/\partial t$ is based on the physical assumption of permanent wave form; this assumption has been discussed in detail by Henderson et al. (2004) and appears to be physically sound when the momentum fluxes are weak, corresponding to the condition that the horizontal linear wave velocity amplitude is much smaller than the wave celerity (see Henderson et al., 2004 for details). If a boundary layer flow quantity ϕ beneath second order Stokes wave forcing can be expressed as

$$\begin{aligned}\phi(x,z,t)=&\,a_1(z)\cos(k_p x-\omega t-\psi_1(z))\\&+a_2(z)\cos 2(k_p x-\omega t-\psi_2(z))\end{aligned} \tag{12}$$

then the relation

$$\frac{\partial \phi}{\partial x}=-\frac{1}{c_p}\frac{\partial \phi}{\partial t} \tag{13}$$

holds; here $c_p=\omega/k_p$, where $k_p=2\pi/\lambda$ is the wave number and ω is the wave frequency. Furthermore, a_1 and a_2 are coefficients and ψ_1 and ψ_2 are phase angles; these quantities are allowed to vary with z. Note that this assumption is possible since the dispersion relation $\omega^2=gk_p\tanh(k_p h)$ is the same for second order Stokes waves as for linear waves (here h is the water depth). Hence the assumption in Eq. (12) is consistent with second order Stokes boundary layer forcing. For linear waves Eq. (13) is valid with $a_2(z)=0$ in Eq. (12).

It should be noted that Eqs. (12) and (13) imply periodic lateral boundary conditions in the physical two-dimensional space. These periodic boundary conditions are justified as a reasonable approximation despite the fact that there will be a small decay of the wave height H due to the dissipation in the boundary layer. This decay can be estimated as

$$\frac{dH}{dx}=-\frac{1}{3}\frac{H^2}{h^2}f_e \tag{14}$$

where f_e is the energy loss factor defined by $\widehat{\tau}_b=0.5\rho f_e\widehat{U}_0^2$ where $\widehat{U}_0$ is the near-bottom horizontal wave velocity amplitude outside the boundary layer, and $\widehat{\tau}_b$ is the bottom shear stress amplitude; see Fredsøe and Deigaard (1992, Chapter 2.5) for a detailed derivation; $f_e=0.00836$ for $A/k_N=1000$ is taken from Table 2.1 in that chapter. Here $A=\widehat{U}_0/\omega$ is the near-bottom wave excursion amplitude. In Section 3 it will be shown that the wave decay is very small for the physical conditions to be discussed.

The lateral periodic boundary conditions is directly related to periodicity in time by Eq. (13); this relation must be applied when the result is mapped from one dimension to the physical two-dimensional space.

2.3. Boundary conditions

2.3.1. At the bottom

The sea bed is assumed to be hydraulically rough. At the theoretical bed level $z_0=k_N/30$ the no-slip condition is applied, i.e.

$$u=0,\quad w=0 \tag{15}$$

For the turbulence field near the bed, the boundary conditions are given in a standard manner (see e.g. Rodi, 1993). By assuming local

equilibrium between production and dissipation, the boundary conditions become

$$k = v_T \left|\frac{\partial u}{\partial z}\right| / \sqrt{c_1} \tag{16}$$

$$\varepsilon = (c_1)^{3/4} \frac{k^{3/2}}{\kappa z_0} \tag{17}$$

where the flow is assumed to be parallel to the wall in the close vicinity of the bottom, i.e. on the computational node nearest the bottom. Here $\kappa = 0.4$. The reference sediment concentration c_a near the sea bed is obtained from the instantaneous Shields parameter θ by the Zyserman and Fredsøe (1994) formula:

$$c_a = \frac{0.331(\theta - \theta_c)^{1.75}}{1 + 0.720(\theta - \theta_c)^{1.75}} \quad \text{at } z = z_a = 2d_{50} \tag{18}$$

2.3.2. At the edge of the boundary layer

As pointed out by Deigaard and Fredsøe (1989) and by Fredsøe and Deigaard (1992, p. 184), the shear stress outside the bottom boundary layer is determined from a balance between the pressure gradient due to the mean surface slope, the radiation stress gradient associated with dissipation of wave energy, and the vertical transfer of momentum caused by the boundary layer streaming. For a specific value of the mean surface slope (the wave set-up) the situation of no shear stress in the water column outside the bottom boundary layer can occur (Deigaard and Fredsøe, 1989; Deigaard et al., 1999). In this case the flow outside the bottom boundary layer can be described by potential theory. This is the situation in nature, which minimizes the drift in the water column outside the bottom boundary layer, representing a physical case of general interest. This situation corresponds to a positive wave-averaged flux of water (over the water depth) which is realistic locally in the open ocean. Near the shore or in a wave flume, it might be more realistic with zero wave-averaged flux of water; this can be obtained by adding a constant adverse horizontal pressure gradient to the time-varying horizontal pressure gradient in Eq. (24). A further discussion on this is given in Deigaard et al. (1999). In the present work the open system situation offshore will be considered. Hence the condition of no shear is applied at the edge of the bottom boundary layer $z = z_{max}$, giving (by using the boundary layer approximation)

$$\frac{\partial u}{\partial z} = 0 \tag{19}$$

This assumption is valid for flows where energy dissipation is taking place only in the near-bed boundary layer. Zero flux conditions are imposed for the turbulent quantities at the edge of the flow domain, giving

$$\frac{\partial k}{\partial z} = 0 \tag{20}$$

$$\frac{\partial \varepsilon}{\partial z} = 0 \tag{21}$$

A zero flux condition is also imposed on the sediment concentration:

$$v_T \frac{\partial c}{\partial z} + w_s c = 0 \tag{22}$$

Following Fredsøe et al. (1985), this vertical flux condition can be simplified; because of the limited vertical extent of the wave boundary layer, Eq. (22) will always degenerate to

$$c \to 0 \quad \text{when } z \to \infty \tag{23}$$

Hence Eq. (23) is implemented at $z = z_{max}$ in the present work. For sheet flow conditions, which will be studied in this work, this boundary condition is consistent.

2.4. Forcing function

Since the boundary layer approximation applies, the horizontal pressure gradient is considered to be constant through the boundary layer. Hence the horizontal pressure gradient $\partial p/\partial x$ is taken from the near-bottom free stream (potential flow) velocity field (U_0, W_0), where U_0 is the horizontal velocity component and W_0 is the vertical velocity component of the free stream velocity. Hence

$$-\frac{1}{\rho}\frac{\partial p}{\partial x} = \frac{\partial U_0}{\partial t} + U_0 \frac{\partial U_0}{\partial x} \tag{24}$$

Here the term $W_0 \partial U_0/\partial z$ has been neglected since both W_0 and $\partial U_0/\partial z$ are small quantities and thus this term is much smaller than the other terms in Eq. (24). In this work the velocity field (U_0, W_0) is given from second order Stokes theory by (see e.g. Dean and Dalrymple, 1991)

$$U_0(x,z,t) = a\frac{gk_p}{\omega}\frac{\cosh(k_p z)}{\cosh(k_p h)}\cos(k_p x - \omega t) + \frac{3}{4}\frac{a^2 \omega k_p \cosh(2k_p z)}{\sinh^4(k_p h)}\cos 2(k_p x - \omega t) \tag{25}$$

$$W_0(x,z,t) = a\frac{gk_p}{\omega}\frac{\sinh(k_p z)}{\cosh(k_p h)}\sin(k_p x - \omega t) + \frac{3}{4}\frac{a^2 \omega k_p \sinh(2k_p z)}{\sinh^4(k_p h)}\sin 2(k_p x - \omega t) \tag{26}$$

Here a is the free surface linear wave amplitude. These free stream velocities are evaluated outside the bottom boundary layer to yield the near-bottom velocities which are forcing the sea bed boundary layer.

2.5. Numerical method and initial conditions

A finite difference method was used to solve the parabolic Eqs. (1), (3), (4), and (9), using second order central differences in space. Geometric stretching of the mesh was applied to obtain a fine resolution close to the bed; a constant stretching factor between 1.08 and 1.10 (depending on the bottom roughness) was applied in the simulations. This grid setting is based on the previous experience when comparing experimental data with simulations. For a given horizontal position beneath the wave, the equations were integrated along vertical lines. Here the vertical mesh was staggered such that the turbulent quantities k and ε are stored at the boundaries of the velocity u cells. The sediment concentration c cells are a subset of the velocity u cells, since the near-bed boundary condition for c is imposed at a given distance above the rough bottom. For each vertical line the spatial discretization of the equations for the horizontal velocity component, turbulent kinetic energy and dissipation rate give a set of stiff differential–integral equations that were integrated simultaneously in time by the integrator VODE (Brown et al., 1989). Then the sediment equation was solved applying the eddy viscosity obtained from the turbulent flow, using the integrator VODE; thus taking advantage of the fact that the velocity is independent of the sediment concentration in the present setting. The integral on the right-hand side of Eq. (11) was evaluated using a trapezoidal method which is consistent with the spatial discretization of the governing equations.

There are no unique initial conditions for this set of parabolic equations, but for any reasonable initial values the solution reaches a steady state solution after a time interval of transients. Thus small positive values of the mean turbulence and flow quantities were initially seeded, and the equations were integrated in time until the flow was fully developed. It should be

noted that the time interval of transients is long for sea bed boundary layers with asymmetric forcing, as shown earlier for horizontally uniform flow by Holmedal and Myrhaug (2006). In order to establish a fully developed flow (in the sense that wave-averaged quantities remain the same after successive wave periods), a spin-up time of 400 wave periods was applied. An extra simulation over 6200 wave periods was carried out to ensure that 400 wave periods of spin-up time was sufficient. Previous experience shows that with this grid structure 100 vertical grid cells are sufficient for resolving the boundary layer. Thus 100 vertical grid cells were used in the simulations. Some simulations with 200 vertical grid cells were carried out with a maximum deviation of 2% for the wave-averaged Eulerian velocities, showing that the grid convergence is sufficient for capturing the steady streaming velocity with a reasonable degree of accuracy.

3. Results and discussion

This paper presents the wave-induced mass transport within the ocean bottom boundary layer for realistic wave conditions, bottom roughnesses, and water depth. Ocean surface waves with an amplitude of $a = 1.22$ m and a period of 6 s propagate over a flat rough bottom. The water depth is 8 m, the resulting wave length is 45 m, and the bottom roughnesses are $z_0 = 1\times10^{-5}$, 3×10^{-5}, 6×10^{-5}, 1×10^{-4}, and 2.3×10^{-4} m. By using the empirical formula $k_N = 2.5d_{50}$, these roughnesses correspond to fine sand, medium sand, coarse sand, very coarse sand, and gravel, respectively (Soulsby, 1997, Chapter 2). This wave condition represents intermediate water depth ($k_p h = 1.11$) with wave steepness $ak_p = 0.17$. The near-bottom potential flow is approximated by second order Stokes theory. This approximation is in accordance with the criterion for which there is no bump in the trough (Dean and Dalrymple, 1991), and Miche's breaking waves criterion (see e.g. Soulsby, 1997). It appears that the no-bump criterion is the most restrictive in this case, corresponding to a maximum wave steepness of $ak_p = 0.22$. In the forthcoming the predictions are conducted with $z_{max} = 0.25$ m. The results given below are for streaming beneath second order Stokes waves unless otherwise specified.

Application of Eq. (14) shows that the wave decay over the wave length is about 2% for $A/k_N = 130$ and less than 1% for $A/k_N = 300$. Thus periodic lateral boundary conditions are reasonable to apply for this case; this is also the case for $A/k_N > 300$ for which the wave decay is smaller due to smaller friction (less rough bottom).

3.1. Mean (wave-averaged) Eulerian velocities and related quantities

Steady streaming in near-bed ocean flows is caused by both wave asymmetry (i.e. by asymmetry of turbulent fluctuations in successive wave half-cycles) as explained by Scandura (2007) and by the presence of a small vertical wave velocity as explained by Longuet-Higgins (1953). It is instructive to isolate the effect of asymmetric forcing, and thus the boundary layer streaming velocity is predicted by neglecting the vertical wave velocity and retaining the asymmetry of the boundary layer forcing. Here the velocity under the wave crest is larger with shorter duration, while the velocity under the wave trough is smaller with longer duration, than for linear waves, causing the resulting steady streaming velocity to become negative as shown in Fig. 1. A similar result was obtained by Scandura (2007) from a direct numerical simulation (DNS) of a horizontally uniform (in terms of mean turbulent quantities) oscillatory boundary layer flow subjected to asymmetric boundary layer forcing. This flow was in the transitional to turbulent flow regime for a flat smooth bottom subjected to infinitesimal disturbances. Scandura (2007) showed that this streaming velocity was caused by the asymmetry of the boundary layer forcing due to different characteristics of the turbulence in successive half-cycles of the periodic (but asymmetric) boundary layer forcing. This leads to a longer duration of the velocity beneath the wave trough than beneath the wave crest. In the present work, which deals with fully rough turbulent flow, the effect of the Reynolds stresses are accounted for by a $(k-\varepsilon)$ eddy viscosity model. In this setting the resulting time-averaged velocity profile depends on the phase difference (during the wave cycle) between the eddy viscosity and the vertical velocity gradient. Some information of the effect of this phase difference can be obtained by splitting both the velocity and the eddy viscosity into a wave-averaged and a periodic part. Following Trowbridge (1983), Davies and Li (1997), and Holmedal and Myrhaug (2006) these quantities are written as

$$u(z,t) = \overline{u(z,t)} + \tilde{u}(z,t)$$
$$\nu_T(z,t) = \overline{\nu_T(z,t)} + \tilde{\nu}_T(z,t)$$

where $\bar{x}$ denotes the time-averaged (over a wave period) component and $\tilde{x}$ denotes the periodic component of the quantity x. Thus the time-averaged shear stress can be decomposed as

$$\overline{\nu_T(\partial u/\partial z)} = \overline{\nu_T}\frac{\partial \overline{u}}{\partial z} + \overline{\tilde{\nu}_T\frac{\partial \tilde{u}}{\partial z}} \tag{27}$$

Here $\rho\overline{\nu_T}\partial\overline{u}/\partial z$ represents the shear stress component associated with the time-averaged flow, and $\rho\overline{\tilde{\nu}_T\partial\tilde{u}/\partial z}$ represents the time-averaged shear stress component caused by the periodic part of the flow. Fig. 2a shows that $\overline{\tilde{\nu}_T\partial\tilde{u}/\partial z}$ is positive and $\overline{\nu_T}\partial\overline{u}/\partial z$ is negative through the boundary layer. Since the eddy viscosity $\overline{\nu_T}$ is always positive, and $\overline{u} = 0$ at the bed, $\overline{\nu_T}\partial\overline{u}/\partial z$ can only be negative if $\overline{u}$ is negative near the bed, indicating a negative near-bed streaming velocity. It should be noted that the wave-averaged shear stress $\overline{\nu_T(\partial u/\partial z)}$ is zero through the boundary layer; this is expected since the wave-averaged of the asymmetric boundary layer forcing is also zero. Davies and Li (1997), Fig. 6 predicted a negative streaming in a horizontally uniform rough turbulent boundary layer subjected to asymmetric forcing using a one-dimensional $k-$model. Experiments conducted by Ribberink and

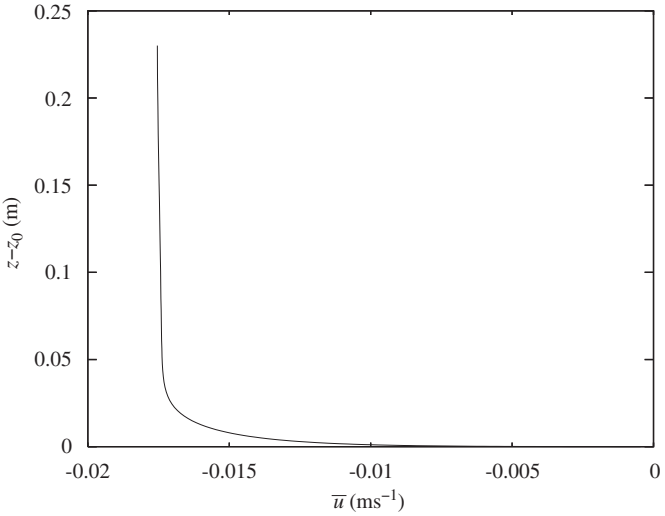

Fig. 1. Mean horizontal boundary layer velocity (i.e. steady streaming velocity) for asymmetric forcing and horizontally uniform velocity (the vertical velocity is zero). Note that the Eulerian and Lagrangian velocities are the same for this particular case with horizontally uniform flow.

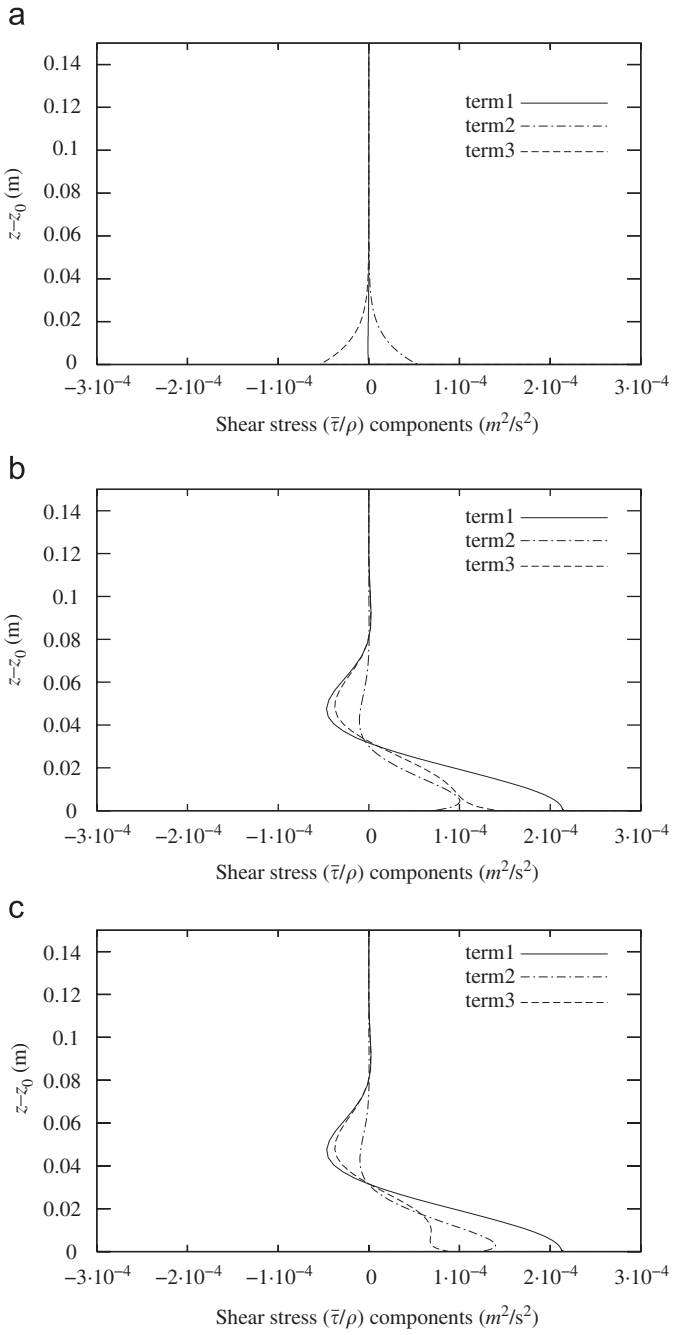

Fig. 2. Mean shear stress $(\overline{\tau}/\rho)$ components: term1 $= \overline{\nu_T \partial u/\partial z}$, term2 $= \overline{\tilde{\nu}_T \partial \tilde{u}/\partial z}$, term3 $= \overline{\nu_T \partial u/\partial z}$. (a) Asymmetric forcing and horizontally uniform flow. (b) Symmetric forcing and vertical velocity included. (c) Asymmetric forcing and vertical velocity included.

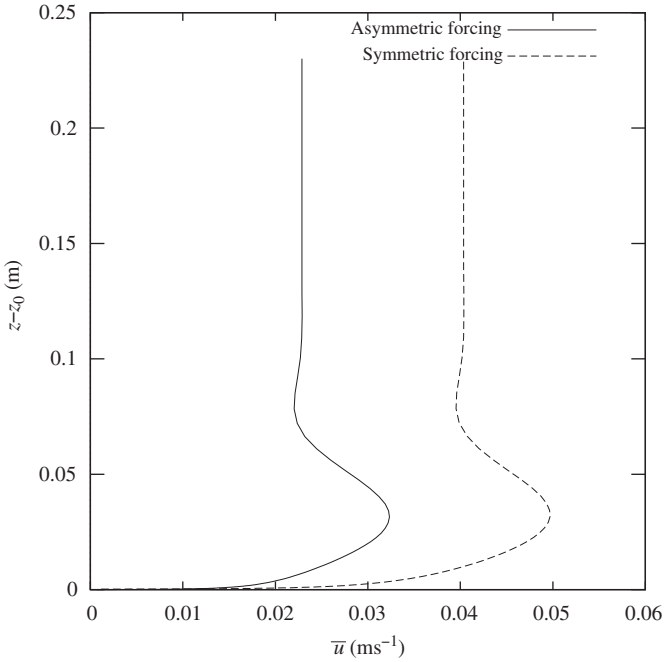

Fig. 3. Mean Eulerian horizontal boundary layer velocity (i.e. steady streaming velocity) for asymmetric and symmetric forcing when the vertical mean turbulent velocity is included.

Al-Salem (1995) in an oscillating water tunnel (horizontally uniform flow) also revealed a negative wave-averaged horizontal velocity near the bottom (see e.g Holmedal and Myrhaug, 2006 for a more detailed discussion). Scandura (2007) obtained a zero wave-averaged velocity for sinusoidal forcing of the horizontally uniform boundary layer; this is also the case with the present predictions. However, when the vertical wave velocity is included (i.e. real propagating waves), the picture becomes more complicated for sinusoidal forcing (Fig. 2b) and second order Stokes forcing (Fig. 2c). Here the wave-averaged shear stress $\overline{\nu_T(\partial u/\partial z)}$ is positive in the vicinity of the bottom. This means that there is a resulting net shear force acting on the bottom when the vertical velocity is included, which have consequences for the bedload transport of sediments as will be shown later.

In real near-bed ocean flows a small vertical wave velocity is always present. Fig. 3 shows that when this vertical velocity is taken into account, the streaming velocity becomes positive (i.e. in the direction of wave propagation) for real sinusoidal and second order Stokes waves, for the present case. This is caused by the term $\partial(\overline{uw})/\partial z$ which acts as a depth-varying force pushing the flow in the direction of wave propagation. Thus the Longuet-Higgins streaming dominates the present case. It is observed that the streaming velocity beneath sinusoidal waves is larger than beneath second order Stokes waves. This means that the effect of asymmetry here is to reduce the streaming. This is physically sound, since the asymmetric forcing for the horizontally uniform boundary layer in Fig. 1 leads to a negative streaming velocity.

Fig. 4a shows $u(t)$ at the edge of the boundary layer for horizontally uniform flow and asymmetric forcing (dashed line) and for a realistic boundary layer flow subjected to asymmetric forcing where the vertical velocity is included (full line), i.e. beneath second order Stokes waves. It appears that for the latter case $u(t)$ is lifted vertically compared to the case of horizontally uniform flow; this is caused by $\partial(\overline{uw})/\partial z$. This 'lifting' leads to a shorter duration of the velocity beneath the wave trough causing the streaming velocity to be in the direction of wave propagation for symmetric forcing. The time series of velocity at the edge of the boundary layer beneath second order Stokes waves is compared with that beneath sinusoidal waves in Fig. 4b. It is observed that asymmetric forcing leads to a larger crest velocity and a lower trough velocity as compared to sinusoidal forcing. Moreover, the duration (in time) of the trough is larger, and the duration of the crest is shorter for asymmetric than for symmetric forcing. This leads to a smaller streaming velocity for asymmetric forcing (i.e. beneath second order Stokes waves) than for symmetric forcing (i.e. beneath sinusoidal waves).

Overall the streaming velocity is caused by both the wave asymmetry and the presence of a vertical wave velocity within the boundary layer, the latter leading to a non-zero $\partial(\overline{uw})/\partial z$. The

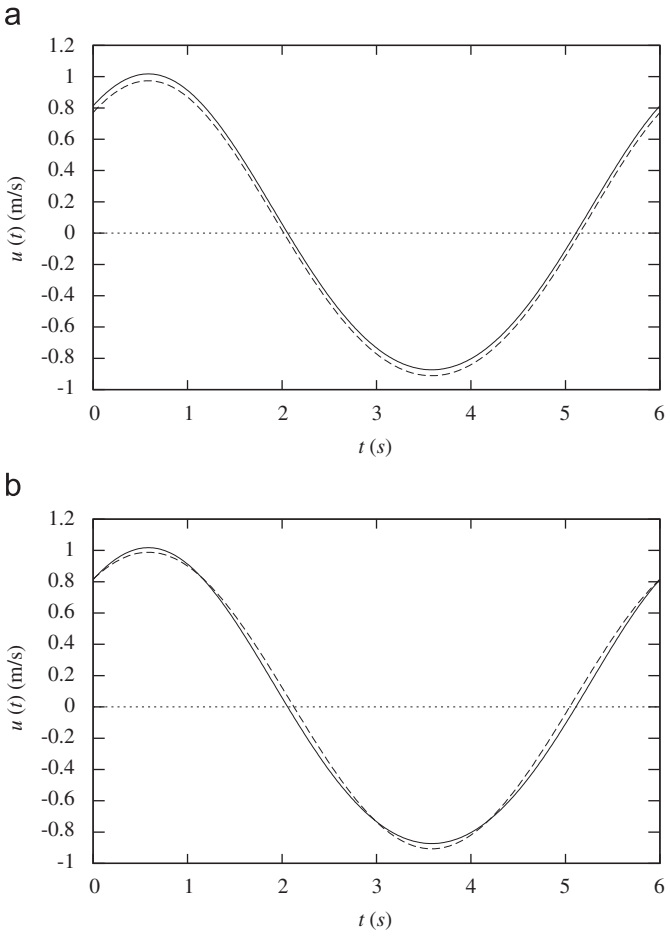

Fig. 4. Mean horizontal Eulerian velocities on the top of the boundary layer. (a) Asymmetric forcing and horizontally uniform flow (dashed line); asymmetric forcing and vertical velocity included (full line). (b) Asymmetric forcing and vertical velocity included (full line); symmetric forcing and vertical velocity included (dashed line).

streaming velocity depends on the interaction between these two contributions. For the present case (as presented in Figs. 1–4) the term $\partial(\overline{uw})/\partial z$ is dominating, leading to a streaming velocity in the direction of wave propagation. However, for longer waves and asymmetric forcing, this term can be very small (since w becomes very small), and the asymmetric turbulence characteristics in successive wave half-cycles might become dominant, leading to a streaming velocity against the wave propagation. Such results will be shown below. This behaviour was first pointed out by Trowbridge (1983) and Trowbridge and Madsen (1984). The result in Fig. 1 is consistent with this result, since horizontally uniform oscillatory flow can be considered as a bottom boundary layer beneath infinitely long waves.

Longuet-Higgins (1953) found that at the edge of the boundary layer the steady streaming velocity (i.e. the wave-averaged horizontal Eulerian velocity) is given by

$$\overline{u}_\infty = \frac{3}{4}\frac{(A\omega)^2}{c_p} \tag{28}$$

Although this result was originally obtained for laminar flow, Longuet-Higgins (1958) showed (in an Appendix to the paper of Russel and Osorio, 1958) that this result is also valid for turbulent flows modelled such that the eddy viscosity is independent of time but allowed to vary vertically. However, Bijker et al. (1974) measured that the steady streaming velocity at the edge of the boundary layer was reduced when the bed roughness was increased for waves propagating over a gently sloping bottom. As pointed out by Trowbridge and Madsen (1984), the rougher beds probably led to higher turbulence intensities, thus indicating that the resulting steady streaming velocity at the edge of the boundary layer is smaller for turbulent flows than for laminar flows. van Doorn (1981) conducted experiments in a wave flume, with waves propagating over a rough bottom. He found that the steady streaming velocity at the edge of the boundary layer was significantly smaller than that obtained by using Longuet-Higgins' result, confirming the indications from Bijker et al. (1974) that the steady streaming velocity at the edge of the boundary layer is reduced for turbulent flows. Unfortunately, the characteristic size of the roughness elements which van Doorn glued to the bottom of the flume is of the same order of magnitude as the near-bottom wave excursion amplitude. Hence form drag becomes important, and this effect is not accounted for in the present model, where the roughness is assumed to affect the turbulence intensity only (taken into account by the average roughness concept). From the experimental findings of Bijker et al. (1974) and van Doorn (1981), it became clear that a time-dependent eddy viscosity was needed to realistically represent steady streaming velocity in rough turbulent oscillatory boundary layers. Later works by, among others, Trowbridge and Madsen (1984) and Brøker (1985) have demonstrated the importance of including a time-variation in the eddy viscosity for oscillating turbulent flows; Trowbridge and Madsen (1984) took the asymmetry of the boundary layer forcing into account, while Brøker (1985) considered sinusoidal boundary layer forcing. Table 1 presents the ratio between the steady streaming velocity at the edge of the boundary layer for the present model and that for the Longuet-Higgins formula for five different bottom roughnesses, represented by $A/k_N = 130$, 300, 600, 1000 and 3000. Results for both sinusoidal (symmetric) and second order Stokes (asymmetric) boundary layer forcing are presented. It appears that for symmetric boundary layer forcing, the ratio is 0.46, while the ratio is 0.26 for asymmetric forcing. Thus the steady streaming velocity at the edge of the boundary layer for rough turbulent oscillatory bottom boundary layers is smaller than that predicted by Longuet-Higgins. It should also be noted that the streaming velocity at the edge of the boundary layer $\overline{u}_\infty$ appears to be almost independent of A/k_N. This is in contradiction to the findings of Brøker (1985) who found a small decrease in $\overline{u}_\infty$ as A/k_N increased.

It is not presently understood why the steady streaming velocity at the edge of the boundary layer is smaller for rough turbulent flows than for laminar flows. It is clear, however, that the effect of the turbulent fluctuations is to modify the mean turbulent flow, also for symmetric boundary layer forcing. Using a time-independent eddy viscosity implies that the Reynolds stresses do not vary with time through the wave cycle, or, by the Boussinesq approximation, that the Reynolds stresses exhibit a time variation exactly equal to that of the vertical mean turbulent velocity gradient (with the present boundary layer

Table 1
Ratio between the steady streaming velocity at the edge of the boundary layer from the present model and from the Longuet-Higgins formula.

A/k_N	Asymmetric forcing	Symmetric forcing
130	0.26	0.45
300	0.26	0.45
600	0.26	0.46
1000	0.26	0.46
3000	0.26	0.46

The Longuet-Higgins formula yields a steady streaming velocity of 0.088 m/s at the edge of the boundary layer.

approximation). Both of these assumptions seem non-realistic, and thus a time-dependent eddy viscosity model is required. When the horizontal velocity is modified by using a time-dependent eddy viscosity model (as in the present $k-\varepsilon$ model) rather than a time-independent eddy viscosity model, the 'lifting' of $u(t)$ caused by $\partial(\overline{uw})/\partial z$ (as described in Fig. 4) may result in different steady streaming velocities at the edge of the boundary layer (due to the different modifications of $u(t)$ by the Reynolds stresses). However, $\partial(\overline{uw})/\partial z$ for laminar flow is not equal to $\partial(\overline{uw})/\partial z$ for rough turbulent flow. It is the interaction between the modification of $u(t)$ by the Reynolds stresses and the effect of $\partial(\overline{uw})/\partial z$ that leads to the resulting steady streaming velocity. This interaction should be further investigated by a DNS of turbulence, but this is beyond the scope of this work.

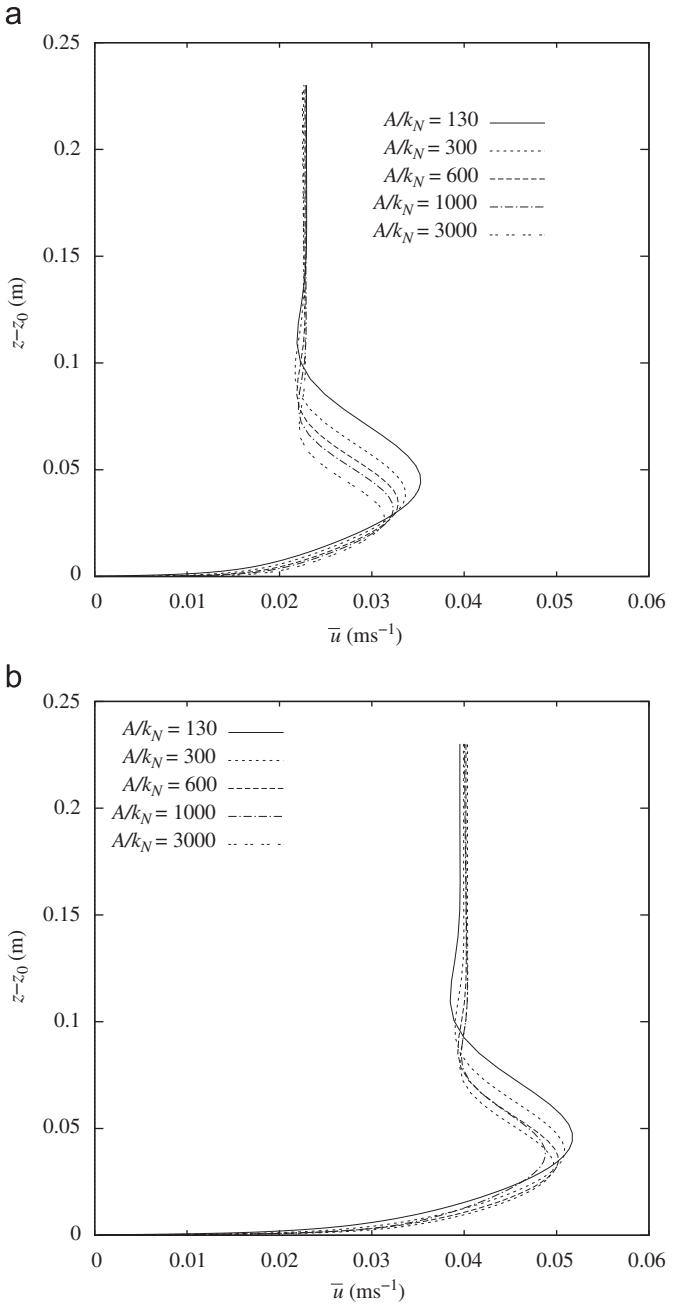

Fig. 5. Mean horizontal Eulerian velocities (i.e. steady streaming velocity) for five different roughness conditions. (a) Asymmetric forcing. (b) Symmetric forcing.

Fig. 5 shows the mean Eulerian horizontal velocity profiles (or steady streaming velocity profiles) for $A/k_N = 130, 300, 600, 1000$, and 3000, for asymmetric (Fig. 5a) and symmetric (Fig. 5b) boundary layer forcing. Here $A/k_N = 130$ represents the largest bottom roughness and$A/k_N = 3000$ represents the smallest bottom roughness. For both cases it is clearly demonstrated that the boundary layer thickness increases as the sea bed roughness increases. It is also demonstrated that the maximum steady streaming velocity within the profile increases as the bottom roughness increases. It is observed that the streaming velocity beneath sinusoidal waves is larger than beneath second order Stokes waves.

Because the horizontal and vertical velocity components are not 90° out of phase within the boundary layer (as they are in potential flow), the product $\overline{uw}$ becomes non-zero, and $\partial(\overline{uw})/\partial z$ imposes a depth-varying force through the boundary layer pushing the water in the direction of wave propagation. The mean product $-\overline{uw}$ beneath second order Stokes waves is shown in Fig. 6 for the five different values of A/k_N. In the close vicinity of the bottom $-\overline{uw}$ is zero as expected, since w approaches zero there. It is also observed that $-\overline{uw}$ at the edge of the boundary layer, $-(\overline{uw})_\infty$, increases as A/k_N decreases. This is expected, since also the bottom shear stress increases as A/k_N decreases, and $-\rho(\overline{uw})_\infty = \overline{\tau}_b$; here $\overline{\tau}_b$ denotes the wave-averaged bottom shear stress. The profile of $-\overline{uw}$ through the boundary layer agrees qualitatively with the corresponding profile obtained by Longuet-Higgins (see e.g. Nielsen, 1992, Fig. 1.4.2), but the magnitude is larger for turbulent flow than for laminar flow.

3.2. *Effect of wave asymmetry and $k_p h$*

The effect of wave asymmetry on the streaming velocities has been investigated by increasing the wave period T_p to 8, 10, and 12 s, keeping all the other physical parameters constant and $A/k_N = 1000$. This leads (via the dispersion relation) to increased wave lengths such that $k_p h$ decreases from 1.1 for $T_p = 6$ s to 0.49 for $T_p = 12$ s. It should be noticed that since A/k_N is constant,

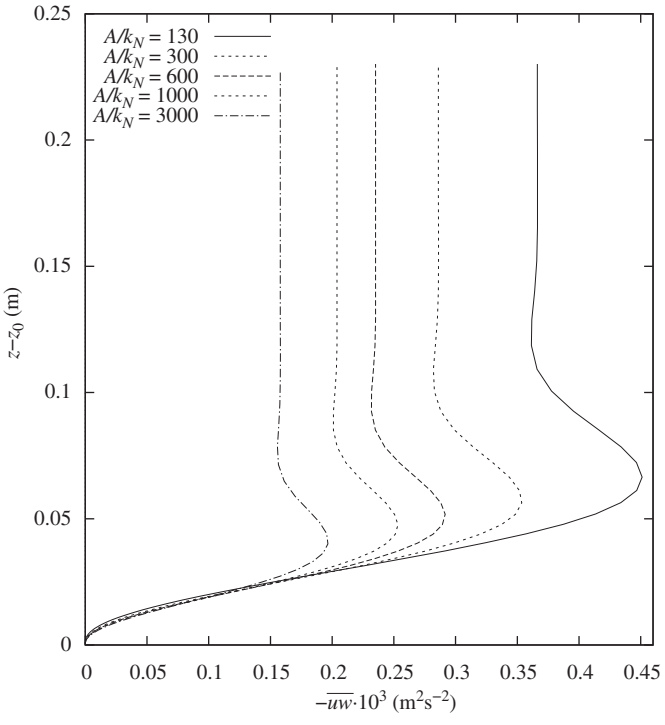

Fig. 6. $-\overline{uw} \times 10^3$ versus $z - z_0$ for five different roughness conditions.

increasing the wave period changes the wave velocity amplitudes, and thereby the asymmetry of the waves. The asymmetry factor R of the waves is defined as

$$R = \frac{U_c}{U_c + U_t} \tag{29}$$

where U_c is the crest velocity outside the boundary layer and U_t is the magnitude of the trough velocity. It should be noted that here it is not possible to isolate the effect of wave asymmetry from the effect of changing $k_p h$. As the wave period (and thereby the wave length) increases, $k_p h$ becomes smaller (implying more shallow water conditions), and the wave asymmetry R increases (for asymmetric forcing). The asymmetry factor R varies from 0.53 for $T_p = 6$ s to 0.58 for $T_p = 12$ s; the details are given in Table 2.

The resulting streaming velocities are shown in Fig. 7. This figure is organized into four rows and three columns: from the upper to the lower row $T_p = 6, 8, 10$, and 12 s, respectively. The left column shows the streaming velocities beneath horizontally uniform asymmetric forcing; the mid column shows the Longuet-Higgins streaming velocities beneath sinusoidal waves, and the right column shows the streaming velocities beneath second order Stokes waves. The difference between the right and the left columns is that the vertical wave velocity is included in the right column (and neglected in the left column).

The left column shows that as T_p increases (and consequently R increases), the negative streaming velocities increases. This is consistent with the findings in Holmedal and Myrhaug (2006) (in the close vicinity of the bottom) for horizontally uniform flows. The mid column shows the Longuet-Higgins streaming velocities; here $R = 0.5$ (sinusoidal waves) and these velocities are always positive. It is observed that these streaming velocities decrease as T_p increases (and thereby $k_p h$ decreases). This is because the ratio between the vertical and horizontal wave velocities becomes smaller as $k_p h$ decreases. Thus the streaming velocities beneath second order Stokes waves depicted in the right column of Fig. 7 is affected by both the increased wave asymmetry and that the wave length becomes larger compared to the water depth as T_p increases (i.e. $k_p h$ decreases). As a result the streaming velocity beneath second order Stokes waves becomes positive (i.e. in the direction of wave propagation) near the bottom and negative at the edge of the boundary layer for $T_p = 8$ s. For $T_p = 10$ and 12 s, the streaming velocity is negative through the entire boundary layer. Fig. 7 clearly shows the effect of wave asymmetry on the streaming velocities beneath second order Stokes waves: subtracting the streaming velocities beneath horizontally uniform asymmetric forcing from the corresponding Longuet-Higgins streaming velocities (which are beneath sinusoidal waves), gives qualitatively the streaming velocities beneath second order Stokes waves. Overall Fig. 7 shows that the streaming velocities beneath second order Stokes waves are affected by two simultaneous effects as the wave period increases: the increase in the asymmetry factor R increases the negative streaming velocities in the left column, and the decrease in $k_p h$ reduces the magnitude of the positive Longuet-Higgins streaming in the mid column. Hence both of these effects reduce the importance of the Longuet-Higgins streaming (i.e. the effect of $\partial(\overline{uw})/\partial z$).

Table 2
Physical parameters for Fig. 7.

Wave period T_p (s)	$k_p h$	R for asymmetric forcing
6	1.11	0.53
8	0.74	0.55
10	0.60	0.56
12	0.49	0.58

The rows in this table correspond to those in Fig. 7.

3.3. Effect on sediment transport

If the wave-induced forcing is strong enough to move the sea bed material (for example sediments and/or pollutants), or to bring it into suspension, then the weak streaming-induced boundary layer drift and non-zero wave-averaged bottom shear stress will cause a net transport of this material over time. This transport may take place either as net transport of suspended sediments or bedload.

Fig. 8 shows the Eulerian wave-averaged suspended sediment flux profiles for Stokes second order wave forcing (Fig. 8a) and sinusoidal forcing (Fig. 8b) for $T_p = 6$ s and for the three median sand grain diameters $d_{50} = 0.13$, 0.21, and 0.32 mm. The corresponding settling velocities are $w_s = 0.0119$, 0.026, and 0.0429 m/s, respectively; these are taken from Dohmen-Janssen et al. (2001). It is observed that the mean sediment flux increases as the median sediment diameter decreases, as expected. It appears that even though the Eulerian streaming velocity is larger beneath sinusoidal waves than beneath second order Stokes waves, the resulting net suspended sediment flux is not very different for the two different forcings, except for $d_{50} = 0.13$ mm, where the flux is larger for sinusoidal waves. The reason for the small difference in suspended sediment flux between asymmetric and symmetric waves for 0.21 mm is shown in Fig. 9, displaying the sediment concentration at 0.5 cm above the bottom through two wave cycles. As the sediment transport results from the dimensionless bottom shear stress (Shields parameter), which is again a result of the boundary layer velocity, the sediment peaks with the longest duration (in time) are those beneath the wave crests, while the sediment peaks with the shortest duration are those beneath the wave troughs. This behaviour is caused by $\partial(\overline{uw})/\partial z$ which gives a 'lift' in the horizontal velocity as discussed previously in conjunction with Fig. 4. Since the shear stress beneath the wave crest is larger for second order Stokes waves than for sinusoidal waves, the corresponding peak value of the sediment concentration is larger for second order Stokes waves than for sinusoidal waves; for the sediment concentration beneath the wave troughs the situation is opposite. This is visualized in Fig. 9; beneath the wave crest (i.e. at the sediment concentration peak with longest duration in Fig. 9) the sediment concentration is higher for second order waves than for sinusoidal waves; beneath the wave trough (i.e. at the sediment concentration peak with shortest duration in Fig. 9) the sediment concentration is lower for second order waves than for sinusoidal waves.

In other words $\partial(\overline{uw})/\partial z$ is responsible for the sediment concentration peaks being 'wide' and 'narrow' beneath the wave crest and the wave trough, respectively; the asymmetry of the boundary layer forcing is responsible for the higher concentration in the 'wide' peak and the lower concentration in the 'narrow' peak, relative to sinusoidal boundary layer forcing. Thus it appears that the integrated effect of asymmetric forcing (relative to sinusoidal forcing) over the wave cycle is small; the higher concentration beneath the wave crests (relative to sinusoidal waves) and the lower concentration beneath the wave troughs tend to almost cancel each other when integrated over the wave cycle, yielding a small contribution to the net suspended sediment flux. Thus it is the Longuet-Higgins streaming effect caused by $\partial(\overline{uw})/\partial z$ being non-zero, which gives the dominating contribution to the net suspended sediment transport. This is quantified in Table 3 which shows the mean suspended sediment transport $\int_{2d_{50}}^{z_{max}} \overline{uc}\, dz$, the mean bedload transport $\overline{q_b}$ and the total sediment transport (the mean suspended sediment transport plus the mean

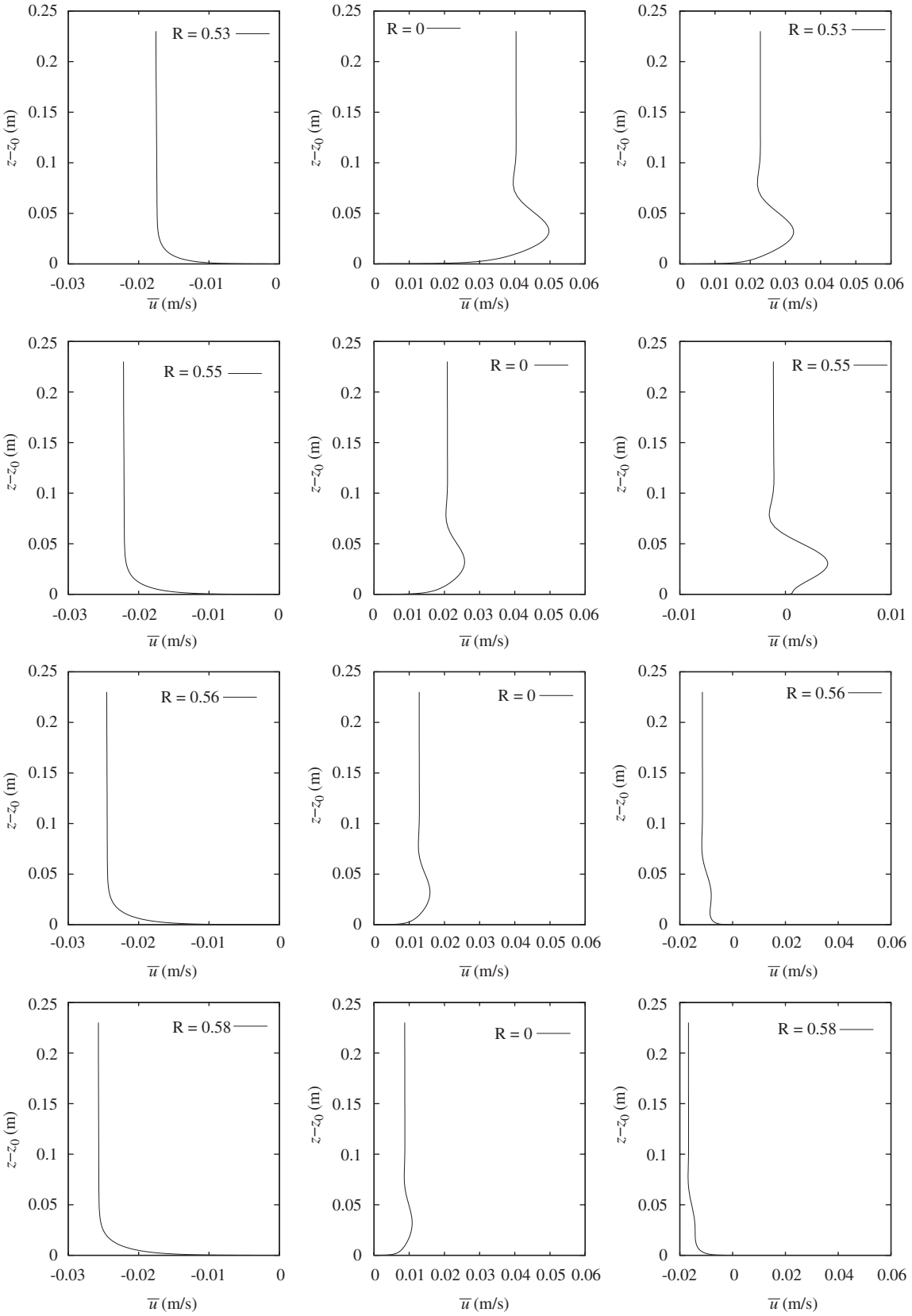

Fig. 7. Streaming velocities for $A/k_N = 1000$ and different wave periods. First row: $T_p = 6$ s, second row: $T_p = 8$ s, third row: $T_p = 10$ s, fourth row: $T_p = 12$ s. The left column shows the streaming velocity beneath horizontally uniform flow as T_p and the asymmetry increases from top towards bottom of the figure: the mid column shows the streaming beneath sinusoidal waves as T_p increases from top towards bottom: the right column shows the streaming beneath second order Stokes waves as T_p and the asymmetry increases from top towards bottom. The asymmetry factor R is given in each subfigure; corresponding values of $k_p h$ are given in Table 2.

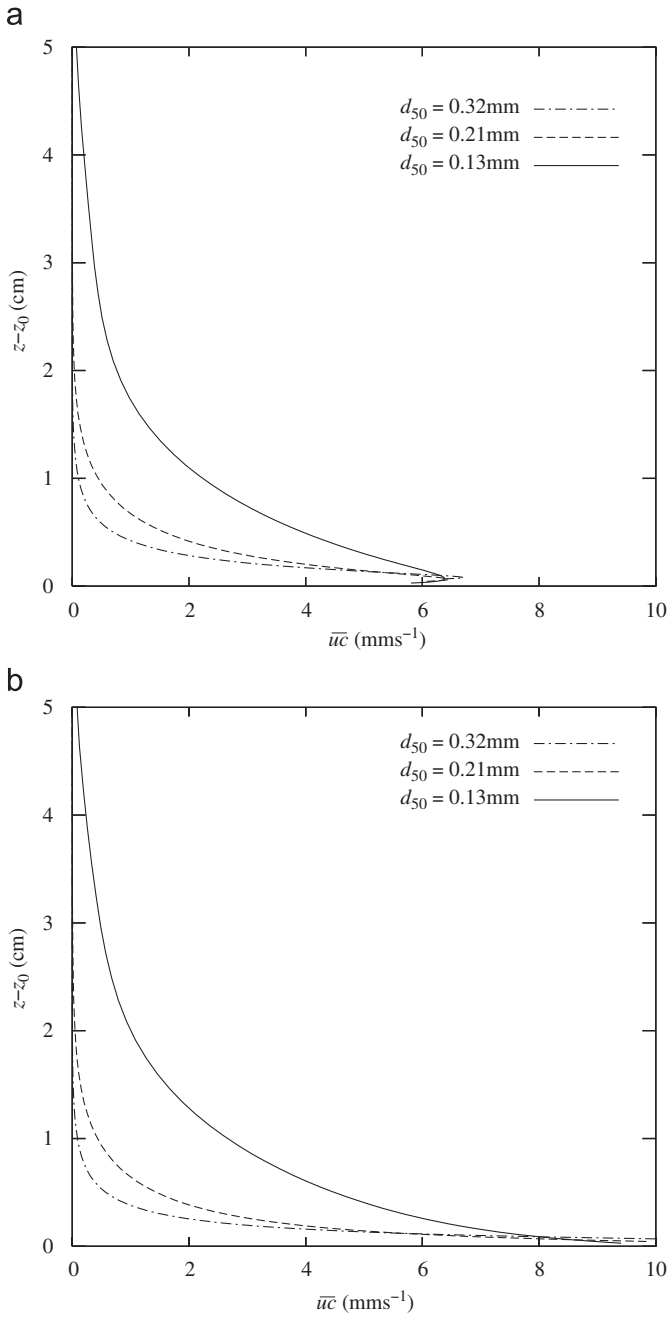

Fig. 8. Wave-averaged sediment flux for three median grain diameters. (a) Asymmetric forcing. (b) Symmetric forcing.

bedload transport). It appears that the total sediment transport beneath second order Stokes waves is not very different from the total sediment transport beneath sinusoidal waves, for 0.21 and 0.32 mm, given the uncertainty which is inherent in these sediment models. For $d_{50} = 0.13$ mm the total sediment transport is larger for sinusoidal waves than for second order Stokes waves. For this case, the total sediment transport is dominated by the net suspended sediment flux and the fact that the streaming velocity beneath sinusoidal waves is larger than beneath second order Stokes waves; fine sediments tend to follow the streaming velocity more closely than the coarser sediments.

Fig. 10 shows the suspended sediment flux profiles for $d_{50} = 0.21$ mm beneath sinusoidal and second order Stokes waves, for wave periods of $T_p = 6$, 8, 10, and 12 s, with the corresponding four different wave asymmetry factors $R = 0.53$, 0.55, 0.56, and 0.58, respectively, and to $k_p h = 1.11$, 0.74, 0.60, and 0.49, respectively. It appears that at a given height above the bottom the suspended sediment flux decreases as T_p increases for both sinusoidal and second order Stokes waves. This is expected, since the streaming velocity decreases as T_p increases, as shown in Fig. 7 (leading to $\overline{uc}$ decreasing). In the close vicinity of the bottom it is observed that the suspended sediment flux beneath second order Stokes waves decreases, and can even be against wave propagation. This is because the phase of the sediment concentration is very close to the phase of the horizontal velocity near the bottom; thus $\overline{uc}$ becomes negative here, since $\overline{u}$ is negative. However, the net suspended sediment flux is in the direction of wave propagation. Table 4 presents the mean suspended sediment transport $\int_{2d_{50}}^{z_{max}} \overline{uc}\, dz$, the mean bedload transport $\overline{q_b}$ and the total sediment transport corresponding to Fig. 10. Overall it appears that the total sediment transport is slightly larger beneath second order Stokes waves than beneath linear waves. The relative difference is largest for the longest wave periods, but here the net sediment transport is very small.

The bedload beneath second order waves is plotted versus time for four different horizontal locations and for $A/k_N = 1000$ and $T_p = 6$ s in Fig. 11. By closer inspection it is observed that the bedload is asymmetric such that the bedload under the wave crest is larger with shorter duration, while the bedload under the wave trough is smaller with longer duration, as for the free stream velocity. It is also visualized that the bedload beneath propagating waves is propagating in space, as expected. It is worth noting that even though the resulting bedload sediment transport within the ocean bottom boundary layer is a second order effect, the cumulative effect on the net transport can be substantial.

Overall, both the suspended sediment transport and the bedload transport are in the direction of wave propagation, even when the streaming velocity is against wave propagation. For the suspended sediment flux the effect of $\partial(\overline{uw})/\partial z$ (as explained above) pushes the suspended sediments in direction of wave

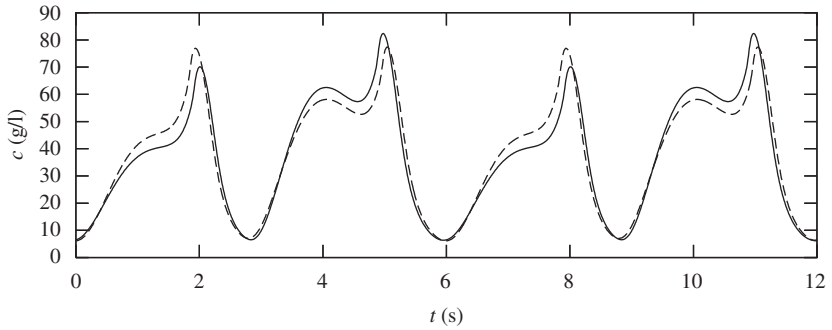

Fig. 9. Sediment concentrations of medium sand ($d_{50} = 0.21$ mm) through two wave cycles at 0.5 cm above the bottom for asymmetric forcing (whole line) and symmetric forcing (dashed line).

Table 3
Mean bedload transport, suspended sediment transport, and total sediment transport ($\overline{q}_{\text{total}}$) for linear waves and Stokes second order waves.

	d_{50} (mm)	$\overline{q_b}$ (mm^2/s)	$\int_{2d_{50}}^{z_{\max}} \overline{uc}\, dz$ (mm^2/s)	$\overline{q}_{\text{total}}$ (mm^2/s)
Linear waves	0.13	8.3	69.8	78.1
Linear waves	0.21	9.2	20.6	29.8
Linear waves	0.32	10.6	11.9	22.5
Stokes second order waves	0.13	10.2	57.9	68.1
Stokes second order waves	0.21	11.5	20.4	31.9
Stokes second order waves	0.32	13.3	12.4	25.7

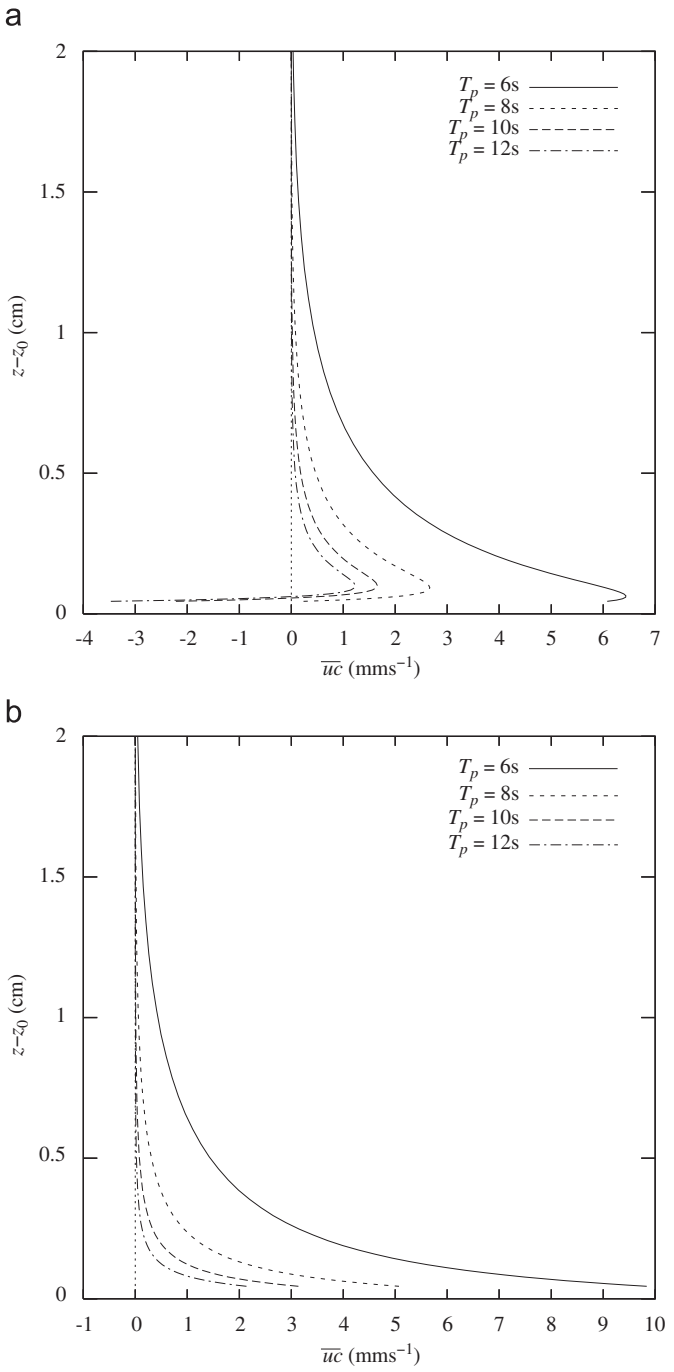

Fig. 10. Wave-averaged sediment flux for $d_{50} = 0.21$ mm and four different wave periods and corresponding wave asymmetry R and $k_p h$ as in Fig. 7. (a) Asymmetric forcing. (b) Symmetric forcing.

propagation. Moreover, the phase difference between the sediment concentration and the horizontal velocity also results in a suspended sediment transport in the wave propagation direction. The bedload transport is a function of the Shields parameter and appears to be in direction of wave propagation. Thus it seems likely that the net sediment transport beneath second order Stokes waves will be in the direction of wave propagation, despite the fact that the streaming velocity can be against wave propagation.

3.4. Lagrangian velocity and particle trajectories

As pointed out by Longuet-Higgins the effect of the water particle trajectories, represented by the Stokes drift, must be taken into account to find the actual mass transport beneath real waves. This will be discussed in the forthcoming. The particle trajectories in the sea bed boundary layer are propagating ellipses. When evaluating the mass transport (i.e. the wave-averaged horizontal Lagrangian velocity) over a wave period, it is necessary to follow the fluid particle along its trajectory through the wave period. For the special case of horizontally uniform flow the mass transport is found by averaging the Eulerian flow field because the particle trajectories do not change in space. For realistic near-bottom flows in the ocean, however, the spatial changes of the particle trajectories must be taken into account (Batchelor, 1967). This is done by a Taylor expansion of the Eulerian flow field (u, w). The result, to second order accuracy, is

$$u_{\mathrm{L}} = u + \left(\int u_{\mathrm{L}}\, dt\right)\frac{\partial u}{\partial x} + \left(\int w_{\mathrm{L}}\, dt\right)\frac{\partial u}{\partial z} \tag{30}$$

$$w_{\mathrm{L}} = w + \left(\int u_{\mathrm{L}}\, dt\right)\frac{\partial w}{\partial x} + \left(\int w_{\mathrm{L}}\, dt\right)\frac{\partial w}{\partial z} \tag{31}$$

where $\int u_{\mathrm{L}}\, dt$ and $\int w_{\mathrm{L}}\, dt$ are the horizontal and vertical displacements, respectively. Here the wave-average of u_{L} (i.e. $\overline{u_{\mathrm{L}}}$) is commonly referred to as the mass transport, representing the mean velocity of a fluid particle averaged over a wave period. It is consistent with second order accuracy to replace u_{L} and w_{L} with u and w in the integrands of Eqs. (30) and (31) (see Mei, 1989, Chapter 9.2 for a detailed outline). Thus the velocity components along the particle trajectories can be evaluated from

$$u_{\mathrm{L}} = u + \left(\int u\, dt\right)\frac{\partial u}{\partial x} + \left(\int w\, dt\right)\frac{\partial u}{\partial z} \tag{32}$$

$$w_{\mathrm{L}} = w + \left(\int u\, dt\right)\frac{\partial w}{\partial x} + \left(\int w\, dt\right)\frac{\partial w}{\partial z} \tag{33}$$

Here the wave-average of the two last terms on the right-hand side of Eq. (32) (i.e. $\overline{(\int u\, dt)\partial u/\partial x} + \overline{(\int w\, dt)\partial u/\partial z}$) is commonly referred to as the horizontal Stokes drift, and $\overline{u}$ is the mean horizontal Eulerian velocity (also denoted the steady streaming velocity). The particle trajectories are found by numerical

Table 4
Mean bedload transport, suspended sediment transport, and total sediment transport ($\overline{q}_{\text{total}}$) for linear waves and Stokes second order waves, for four different wave periods and corresponding values of wave asymmetry R and $k_p h$; here $d_{50} = 0.21$ mm.

	T_p (s)	$k_p h$	R	$\overline{q_b}$ (mm^2/s)	$\int_{2d_{50}}^{z_{max}} \overline{uc}\, dz$ (mm^2/s)	$\overline{q}_{\text{total}}$ (mm^2/s)
Stokes 2nd order waves	6	1.11	0.53	11.5	20.4	31.9
Stokes 2nd order waves	8	0.74	0.55	4.3	6.9	11.2
Stokes 2nd order waves	10	0.60	0.56	2.3	3.2	5.5
Stokes 2nd order waves	12	0.49	0.58	1.5	1.8	3.3
Linear waves	6	1.11	0.50	9.2	20.6	29.8
Linear waves	8	0.74	0.50	2.6	6.0	8.6
Linear waves	10	0.60	0.50	0.98	2.5	3.48
Linear waves	12	0.49	0.50	0.44	1.24	1.68

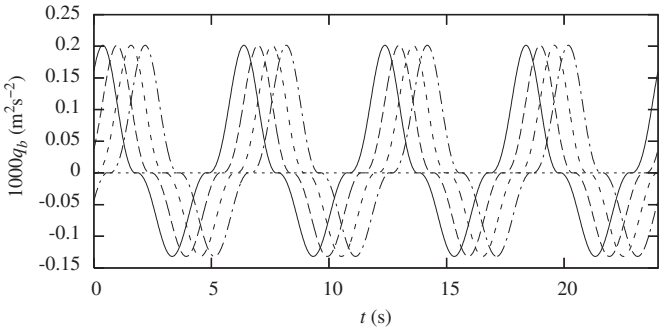

Fig. 11. Bedload at $A/k_N = 1000$ for four different horizontal locations: From left to right: $x/\lambda = 1/8$ (whole line), $x/\lambda = 1/4$ (long-dashed line), $x/\lambda = 3/8$ (short-dashed line), and $x/\lambda = 1/2$ (dash-dotted line).

integration of Eqs. (32) and (33) in time, using Eq. (13) and following the particles in a Lagrangian sense.

Fig. 12 shows particle trajectories at different vertical elevations within the boundary layer through four wave periods, for $A/k_N = 1000$ and $T_p = 6$ s and for a fixed horizontal location ($x/\lambda = 0.1$). Here the boundary layer is subjected to second order Stokes forcing. The water particles move in ellipses that flatten as the sea bed is approached, as expected (Fig. 12a). The time lag vertically through the boundary layer and the characteristic horizontal velocity overshoot are clearly visualized (by following vertically each symbol which marks the end of a wave cycle in the figure). It is also noticed that even very close to the bed, the vertical velocity is non-zero (Fig. 12b). The particle trajectories do not close; they propagate the same distance during each wave period, resulting in propagating ellipses. This visualizes the resulting mass transport within the sea bed boundary layer; i.e. the mass transport velocity equals the distance which these ellipses propagate during one wave period divided by the same wave period.

Fig. 13 shows the mass transport velocity (i.e. the wave-averaged Lagrangian velocity) profiles for $A/k_N = 130$, 300, 600, 1000, and 3000, for asymmetric (Fig. 13a) and symmetric (Fig. 13b) boundary layer forcing with $T_p = 6$ s. For both cases it is clearly demonstrated that the mass transport is in the direction of wave propagation for this physical choice of parameters, and that it is larger beneath sinusoidal waves than beneath second order Stokes waves. It is also observed that the boundary layer thickness increases as the sea bed roughness increases, and that the maximum mass transport through the profile increases as the bottom roughness increases. As for the case of the steady streaming velocity profiles in Fig. 5, the mass transport velocity at the edge of the boundary layer $\overline{u}_{L,\infty}$ appears to be almost independent of A/k_N. Longuet-Higgins (1958) found that at the edge of the boundary layer the horizontal mass transport velocity

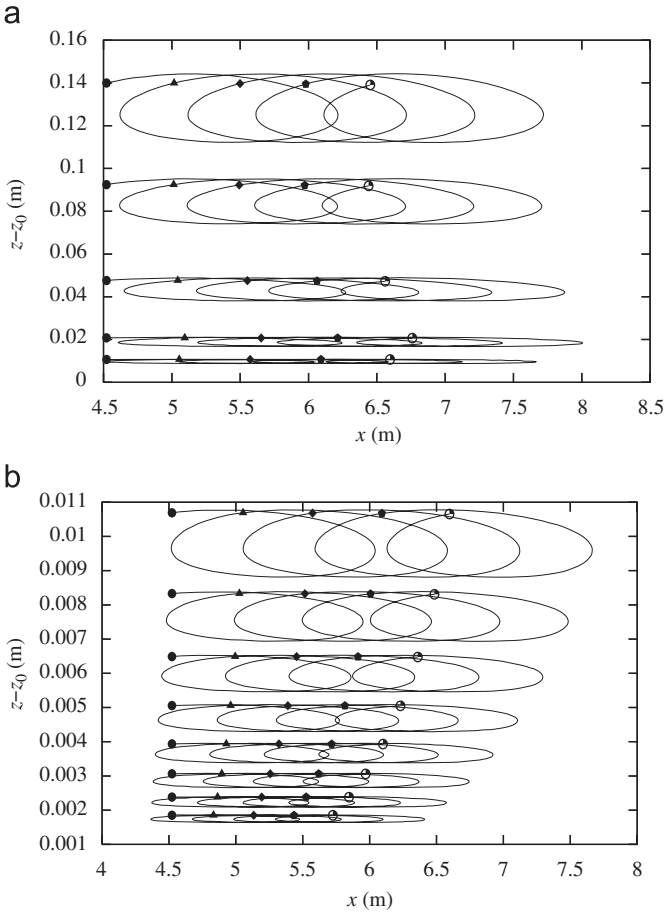

Fig. 12. Particle trajectories at $x/\lambda = 0.1$ for $A/k_N = 1000$. (a) View of boundary layer from the bottom. (b) Close-up in the lower region. The five symbols from left towards right for each particle trajectory are such that the first symbol denotes the start point; the second to fifth symbol denotes the points after one to four wave periods, respectively.

is given by

$$\overline{u}_{L,\infty} = \frac{5}{4}\frac{(A\omega)^2}{c_p} \tag{34}$$

which is valid for laminar flow and for turbulent flows modelled such that the eddy viscosity is independent of time but allowed to vary vertically. Hence the Longuet-Higgins steady streaming velocity $\overline{u}_\infty$ in Eq. (28) is 60% of the corresponding mass transport velocity $\overline{u}_{L,\infty}$. Table 5 shows the ratio between the mass transport velocity at the edge of the boundary layer for the present model and that for the Longuet-Higgins formula for five different bottom

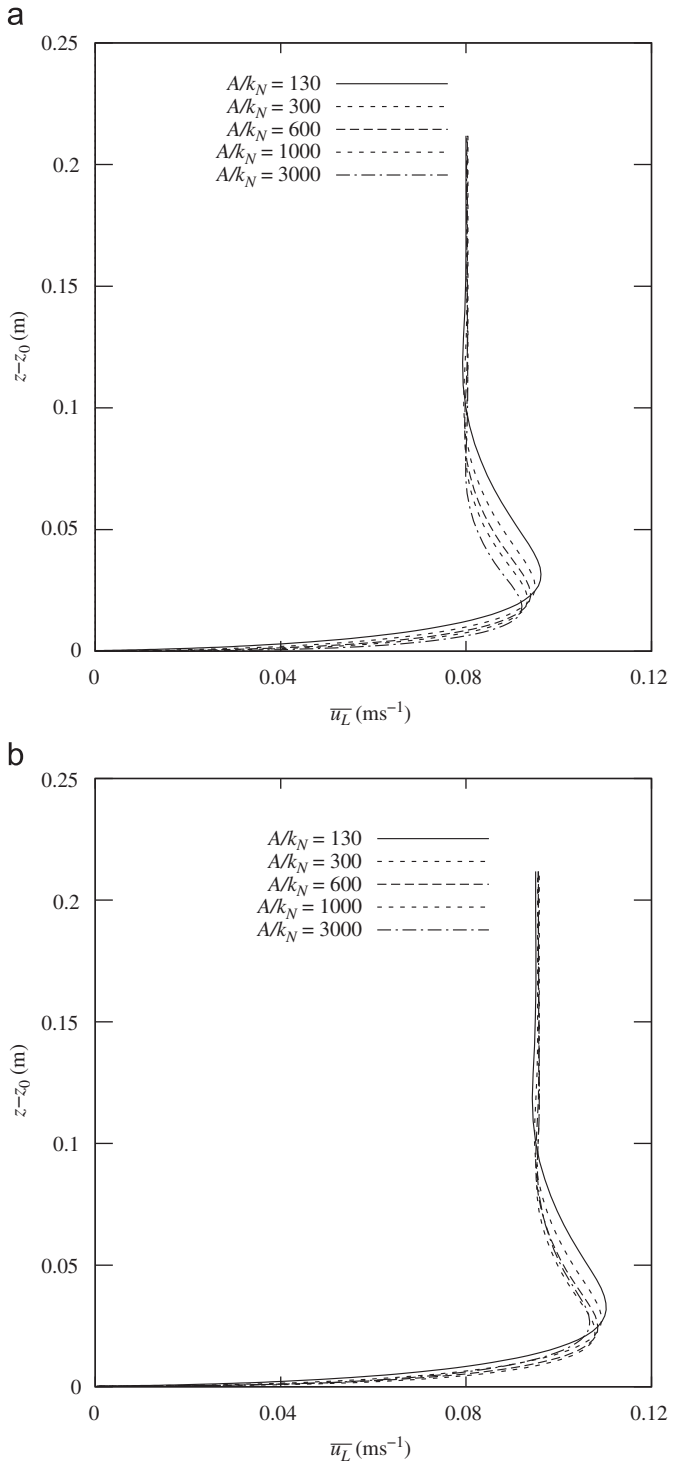

Fig. 13. Mean mass transport velocities (i.e. wave-averaged Lagrangian velocities) for five different roughness conditions. (a) Asymmetric forcing. (b) Symmetric forcing.

roughnesses, represented by $A/k_N = 130$, 300, 600, 1000, and 3000. Results for both sinusoidal and asymmetric boundary layer forcing are presented. It appears that for sinusoidal boundary layer forcing, the ratio is 0.65, while the ratio is 0.54 when the boundary layer is driven by second order Stokes waves forcing. Thus the steady streaming velocity at the edge of the boundary layer for rough turbulent oscillating bottom boundary layers is smaller than that predicted by Longuet-Higgins.

Table 5
Ratio between mass transport velocity at the edge of the boundary layer from the present model and from the Longuet-Higgins formula.

A/k_N	Asymmetric forcing	Symmetric forcing
130	0.55	0.65
300	0.55	0.65
600	0.54	0.65
1000	0.54	0.65
3000	0.54	0.65

The Longuet-Higgins formula yields the mass transport velocity 0.147 m/s at the edge of the boundary layer.

It is of interest to compare the present mass transport at the edge of the boundary layer with the corresponding horizontal Stokes drift velocity $\overline{u}_s = (g(ak_p)^2)/(\omega \sinh(2k_p h))$ (evaluated at the bottom) which exists in potential flow due to the fact that the water particles move faster beneath the crests than beneath the troughs. At the edge of the boundary layer $\overline{u}_{L,\infty} = 1.36\overline{u}_s$ for second order Stokes forcing; $\overline{u}_{L,\infty} = 1.54\overline{u}_s$ for linear (sinusoidal) forcing. Thus the mass transport velocity at the edge of the boundary layer is larger than that obtained by the Stokes drift from potential theory where the boundary layer is neglected.

Fig. 14 shows the mass transport velocity (i.e. the wave-averaged Lagrangian velocity) profiles for wave periods $T_p = 6$, 8, 10, and 12 s, corresponding to four different wave asymmetries R and values of $k_p h$ as in Fig. 10. Here $A/k_N = 1000$ and thus these physical parameters are the same as those presented in Fig. 10. It is observed in Fig. 14b that the mass transport beneath sinusoidal waves decreases as the wave length to water depth ratio increases (i.e. $k_p h$ decreases). This is expected due to the similar behaviour of the Eulerian wave averaged velocities as shown in Fig. 7. It is interesting to note that the mass transport beneath second order Stokes waves can be almost zero for sufficiently long waves (for a fixed water depth) and large enough wave asymmetry (Fig. 14a). Hence the effect of wave asymmetry is to drastically reduce the mass transport compared to sinusoidal waves.

4. Summary and conclusions

The interaction between two important mechanisms which causes streaming has been investigated by numerical simulations of the seabed boundary layer beneath both sinusoidal waves and Stokes second order waves, as well as horizontally uniform bottom boundary layers with asymmetric forcing. These two mechanisms are streaming caused by turbulence asymmetry in successive wave half-cycles (beneath asymmetric forcing), and streaming caused by the presence of a vertical wave velocity within the seabed boundary layer as earlier explained by Longuet-Higgins. The effect of wave asymmetry, wave length to water depth ratio, and bottom roughness have been investigated for realistic physical situations. The streaming induced sediment dynamics near the ocean bottom has been investigated; both the resulting suspended load and bedload are presented. Finally, the mass transport (wave-averaged Lagrangian velocity) has been studied for a range of wave conditions. The main results are as follows:

- Steady streaming in near-bed ocean flows is caused by both wave asymmetry (by asymmetry of turbulent fluctuations in successive wave half-cycles) and by the presence of a small vertical wave velocity in the boundary layer (Longuet-Higgins streaming). The steady streaming results from an interaction

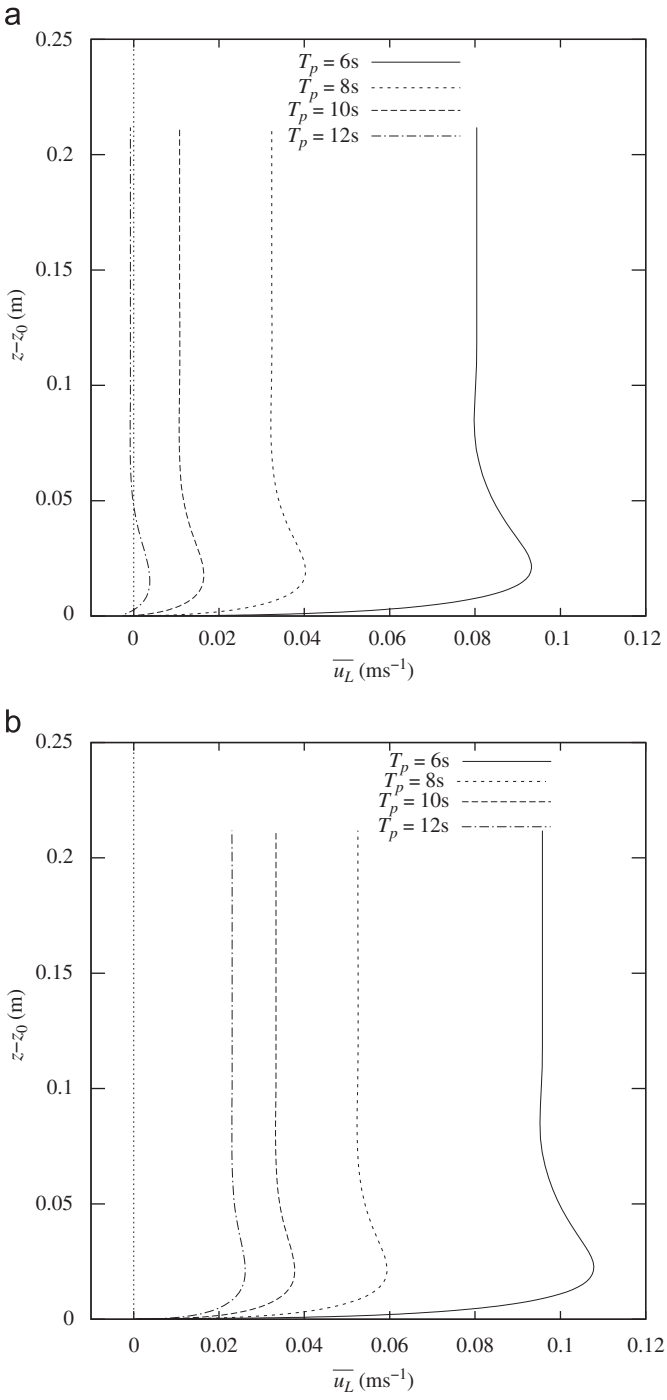

Fig. 14. Mean mass transport velocities (i.e. wave-averaged Lagrangian velocities) for $A/k_N = 1000$ and four different wave periods. The wave periods and the corresponding values of $k_p h$ and R are given in Table 2. (a) Asymmetric forcing. (b) Symmetric forcing.

between these two effects; this interaction depends on the degree of wave asymmetry and how long the waves are compared to the water depth. The Longuet-Higgins streaming decreases as the wave length increases for a given water depth, and the effect of wave asymmetry can dominate, leading to a steady streaming against the wave propagation.

- The streaming velocities beneath sinusoidal waves (Longuet-Higgins streaming) is always in the direction of wave propagation, while the streaming velocities in horizontally uniform boundary layers with asymmetric forcing are always negative. Thus the effect of asymmetry in second order Stokes waves is either to reduce the streaming velocity in the direction of wave propagation, or, for long waves relative to the water depth, to induce a streaming velocity against the direction of wave propagation.
- The asymmetry of second order Stokes waves reduces the mass transport (wave-averaged Lagrangian velocity); for a fixed water depth this mass transport can become almost zero for sufficiently long waves and large enough wave asymmetry.
- An increase in the bottom roughness leads to an increase in the boundary layer thickness, the maximum steady streaming velocity, and mass transport velocity within the boundary layer. The steady streaming velocity and mass transport velocity at the edge of the boundary layer do not seem to vary much with the bottom roughness.
- The boundary layer streaming leads to a wave-averaged transport of suspended sediments and bedload in the direction of wave propagation. The Longuet-Higgins streaming is the dominating mechanism acting on the sediments, and thus the total sediment transport is not very different beneath sinusoidal waves and second order Stokes waves. This is the case except for fine sediments, where the total sediment transport is dominated by suspension, i.e. the larger streaming velocity beneath symmetric waves results in larger suspended sediment transport beneath sinusoidal waves than beneath second order Stokes waves.

Acknowledgement

This work was carried out as a part of the project 'Wave-Current Interactions and Transport Mechanisms in the Ocean' funded by the Norwegian Research Council. This support is gratefully acknowledged.

References

Batchelor, G.K., 1967. An Introduction to Fluid Dynamics. Cambridge University Press, Cambridge.
Bijker, E.W., Kalkwijk, J.P.T., Pieters, T., 1974. Mass transport in gravity waves on a sloping bottom. In: 14th International Conference on Coastal Engineering, Copenhagen, pp. 24–28.
Brøker, I.H., 1985. Wave generated ripples and resulting sediment transport in waves, Series paper no. 36. Institute of Hydrodynamics and Hydraulic Engineering, ISVA, Techn. University of Denmark.
Brown, P.N., Byrne, G.D., Hindmarsh, A.C., 1989. VODE: a variable coefficient ODE solver. SIAM Journal on Scientific and Statistical Computing 10, 1038–1051.
Chowdhury, A.C., Sato, M., Ueno, A., 1997. Numerical model of the turbulent wave boundary layer induced by finite amplitude water waves. Applied Ocean Research 19, 201–209.
Collins, J.I., 1963. Inception of turbulence at the bed under periodic gravity waves. Journal of Geophysical Research 68, 6007–6014.
Davies, A.G., Li, Z., 1997. Modelling sediment transport beneath regular symmetrical and asymmetrical waves above a plane bed. Continental Shelf Research 17 (5), 555–582.
Dean, R.G., Dalrymple, R.A., 1991. Water wave mechanics for engineers and scientists. In: Advanced Series on Ocean Engineering, vol. 2. World Scientific, Singapore.
Deigaard, R., Fredsøe, J., 1989. Shear stress distribution in dissipative water waves. Coastal Engineering 13, 357–378.
Deigaard, R., Jacobsen, J.B., Fredsøe, J., 1999. Net sediment transport under wave groups and bound long waves. Journal of Geophysical Research 104 (C6), 13559–13575.
Dohmen-Janssen, C.M., Hassan, W.N., Ribberink, J.S., 2001. Mobile-bed effects in oscillatory sheet flow. Journal of Geophysical Research 106 (C11), 27103–27115.
Fredsøe, J., 1984. Turbulent boundary layer in wave-current motion. Journal of Hydraulic Engineering—ASCE 110, 1103–1120.
Fredsøe, J., Anderson, O.H., Silberg, S., 1985. Distribution of suspended sediment in large waves. Journal of Waterway, Port, Coastal Ocean Engineering 111, 1041–1059.
Fredsøe, J., Deigaard, R., 1992. Mechanics of Coastal Sediment Transport. World Scientific, Singapore.
Henderson, S.M., Allen, J.S., Newberger, P.A. 2004. Nearshore sandbar migration predicted by an eddy-diffusive boundary layer model. Journal of Geophysical Research, 109, C06024.

Holmedal, L.E., Myrhaug, D., 2006. Boundary layer flow and net sediment transport beneath asymmetrical waves. Continental Shelf Research 26, 252–268.
Holmedal, L.E., Myrhaug, D., Eidsvik, K.J., 2004. Sediment suspension under sheet flow conditions beneath random waves plus current. Continental Shelf Research 24, 2065–2091.
Holmedal, L.E., Myrhaug, D., Rue, H., 2003. The sea bed boundary layer under random waves plus current. Continental Shelf Research 23 (7), 717–750 erratum 1035.
Hsu, T.W., Ou, S.H., 1994. On the mass transport of water waves in a turbulent boundary layer. Ocean Engineering 21 (2), 195–206.
Jensen, B.L., Sumer, B.M., Fredsøe, J., 1989. Turbulent oscillatory boundary layers at high Reynolds numbers. Journal of Fluid Mechanics 206, 265–297.
Johns, B., 1977. Residual flow and boundary shear stress in the turbulent bottom layer beneath waves. Journal of Physical Oceanography 7, 733–738.
Justesen, P., 1988. Turbulent wave boundary layers, Series paper no. 43. Technical University of Denmark, Institute of Hydrodynamics and Hydraulic Engineering.
Justesen, P., 1991. A note on turbulence calculations in the wave boundary layer. Journal of Hydraulic Research 29, 699–711.
Launder, B.E., Spalding, D.B., 1974. The numerical computation of turbulent flows. Computer Methods in Applied Mechanics and Engineering (3), 269–289.
Longuet-Higgins, M.S., 1953. Mass transport in water waves. Philosophical Transactions of the Royal Society of London Series A 245, 535–581.
Longuet-Higgins, M.S., 1958. The mechanics of the boundary layer near the bottom in a progressive wave. Appendix to 'An experimental investigation of drift profiles in a closed channel' by R.C.H. Russel and J.D.C Osorio. In: Proceedings of the 6th International Conference on Coastal Engineering, ASCE, Miami, pp. 184–193.
Mei, C.C., 1989. The Applied Dynamics of Ocean Surface Waves, second ed. Advanced Series on Ocean Engineering, vol. 1, World Scientific, Singapore.
Nielsen, P., 1992. Coastal Bottom Boundary Layers and Sediment Transport. World Scientific, Singapore.
Ribberink, J.S., Al-Salem, A.A., 1995. Sheet flow and suspension of sand in oscillatory boundary layers. Coastal Engineering 25, 205–225.
Riley, N., 2001. Steady streaming. Annual Review of Fluid Mechanics 33, 43–65.
Rodi, W., 1993. Turbulence Models and Their Application in Hydraulics, A state-of-the-art Review. IAHR Monograph Series, third ed. A.A. Balkema, Rotterdam, Netherlands.
Russel, R.C.H., Osorio, J.D.C., 1958. An experimental investigation of drift profiles in a closed channel. In: Proceedings of the 6th International Conference on Coastal Engineering, ASCE, Miami, pp. 171–193.
Scandura, P., 2007. Steady streaming in a turbulent oscillating boundary layer. Journal of Fluid Mechanics 571, 265–280.
Soulsby, R.L., 1997. Dynamics of Marine Sands. Thomas Telford Publications.
Trowbridge, J.H., 1983. Wave-induced turbulent flow near a rough bed: implications of a time-varying eddy viscosity. Ph.D. Thesis, MIT and Woods Hole Oceanographic Institution.
Trowbridge, J., Madsen, O.S., 1984. Turbulent wave boundary layers 2. Second-order theory and mass transport. Journal of Geophysical Research 89 (C5), 7999–8007.
van Doorn, T., 1981. Experimental investigation of near-bottom velocities in water waves without and with a current. Report of investigations M1, Delft Hydraulics Laboratory.
Zyserman, J.A., Fredsøe, J., 1994. Data analysis of bed concentration of suspended sediment. Journal of Hydraulic Research 120 (9), 1021–1042.